RSC Advances

ROYAL SOCIETY OF CHEMISTRY

www.rsc.org/advances

Journal Name

ARTICLE

Highly efficient photocatalytic hydrogen generation by incorporating CdS into ZnCr-layered double hydroxide interlayer†

Guohua Zhang, Bizhou Lin,* Weiwei Yang, Shaofeng Jiang, Qianru Yao, Yilin Chen and Bifen Gao

CdS-pillared ZnCr-LDH nanohybrid was prepared through incorporating CdS nanoparticles into the interlayer of ZnCr-LDH nanosheets *via* an exfoliation-restacking route. The resultant nanohybrid exhibits an interlayer spacing of 2.50 nm and a mesoporous texture with a specific surface area of 86 m^2 g^{-1}. It was revealed that there exists a strong electronic coupling between the two components in the pillared heterostructure, which remarkably suppresses the photogenerated electron-hole recombination. The as-prepared nanohybrid displayed significantly enhanced photocatalytic activity. Its H_2-evolution rates were as high as 374 $\mu mol \cdot h^{-1} \cdot g^{-1}$ with a quantum efficiency of 42.6% and 2164 $\mu mol \cdot h^{-1} \cdot g^{-1}$ with a quantum efficiency of 48.2% under visible and UV-visible light, respectively, which were far superior to those of its parents ZnCr-LDH and CdS. The present findings clearly demonstrate that the self-assembly of CdS-LDHs is quite effective in synthesizing novel LDHs-based visible-light-driven photocatalysts with high performance in hydrogen evolution from water splitting.

1. Introduction

Confronting the increasingly serious energy crisis and the environmental pollution caused by the burning of fossil fuels, the research and development of renewable and environmental-friendly energy recourses has attracted extensive attention.[1] One of the most effective approaches is to convert solar energy into clean energy, achieving through the photoinduced production of H_2 molecules from water by semiconductor photocatalysts.[1–4] Since the ultraviolet light only accounts for about 4% of the solar energy and the visible light contributes to about 43%, it is important to develop visible-light-driven photocatalysts.[4–6] Compared with many oxides, cadmium sulfide (CdS) possesses a relatively narrow bandgap, which can efficiently absorb visible light, and a conduction band edge sufficiently more negative than the reduction potential of protons, which endows CdS to have a high photoactivity for H_2 evolution under visible-light irradiation.[7,8]

However, during the photocatalytic process, CdS particles tend to aggregate into larger particles, which leads to a bad

recurrence and a high recombination of electron–hole pairs.[4,8] To overcome these limitations, scientists have explored many approaches to enhance the photocatalytic activity of CdS, including deposition of noble metals,[9,10] modification with carbon nanomaterials,[11–13] and formation of heterojunction semiconductors.[14,15] It was notable that incorporating CdS particles into the interlayer and the surface of titanate can efficiently suppress the growth of semiconductor particles as well as facilitate the transfer of the photogenerated electrons to the surface of photocatalysts, resulting in a high photocatalytic efficiency.[16]

Layered double hydroxides (LDHs), a large class of two-dimensional (2D) anionic clays, are made up of positively charged brucite-like layers and exchangeable interlayer anions with a general formula of $[M^{2+}_{1-x}M^{3+}_x(OH)_2](A^{n-})_{x/n} \cdot mH_2O$. LDHs have been widely used as heterogeneous catalysts for base-catalyzed reactions or redox transformations.[17–20] However, the photocatalytic properties of LDHs have been mostly ignored.[17,21] García et al. firstly reported the high photocatalytic activity of ZnCr-LDH for visible light-induced O_2 generation,[22] which provides a fresh perspective for exploring new LDH-based photocatalysts. Some high efficient LDHs-based photocatalysis for O_2 evolution were later found, such as NiTi-LDH [23] and ZnCr-LDH/graphene,[24] ZnCr-LDH/layered titanate,[2] ZnCr-LDH/polyoxometates,[25] and NiTi-

Fujian Key Laboratory of Functional Materials, College of Materials Science and Engineering, Huaqiao University, Xiamen 361021, P. R. China. E-mail address: bzlinhqu@126.com; Fax: +86-592-6162221.

LDH/graphene composites.[26] Nevertheless, there are only a few reports about photocatalytic water splitting into H_2 based on LDHs. Very recently, Parida and coworkers reported that the carbonate intercalated ZnCr-LDH,[27] and ternary Mg(Al+Fe)- and (Ni+Zn)Cr-LDHs have good photocatalytic activity towards hydrogen evolution from water.[21,28]

In recent years, one of the hotspots in photocatalysis is incorporating oxide-semiconductor nanoparticles into the interlayer of layered metal semiconductors to form pillared nanohybrids, such as $TiO_2/HTiNbO_5$,[29] $CrO_x/Ti_{1.83}O_4$,[30] and $TiO_2/Nb_{6-x}Bi_xO_{17}$.[31] These materials have been prepared through the exfoliation–restacking technology,[29–31] which is feasible to insert a big dimension guest as the pillar material into the interlayer spacing of the layered host solid. The formed heterojunctions resulted in the spatial separation of photoinduced electrons and holes, which effectively inhibits the recombination between the photogenerated charge carriers and improves the photocatalytic efficiency. It was demonstrated that the action of formamide on LDHs can induce their exfoliation into positively charged unilamellar nanosheets,[17,32] which indicates the LDH-based pillared nanohybrids can be prepared by electrostatically derived self-assembly in the presence of negatively charged nanoparticles. The previous CdS-pillared LDHs were synthesized by an organically pre-expanded templating method or an ion-exchange and a subsequent sulfurization process.[33,34] However, this type of material is not so effective for H_2 production.[16] In the present study, we have developed the exfoliation–restacking technology to prepare a novel CdS-pillared ZnCr-LDH. The present heterostructured nanohybrid is mesoporous and exhibits high photocatalytic activity for H_2 generation from water splitting.

2. Experimental

2.1 Synthesis of photocatalysts

All the reagents were of analytical-grade and were used as received without further purification. The pristine ZnCr-LDH in the nitrate form was prepared by the hydrothermal method, similar to the reported procedure.[35] Firstly, under the protection of N_2 atmosphere, a mixture of $Zn(NO_3)_2 \cdot 6H_2O$, $Cr(NO_3)_3 \cdot 9H_2O$ and $NaNO_3$ with Zn/Cr/NO_3 molar ratio 2:1:1 was dissolved in 100 ml of decarbonated deionized water ($[Zn^{2+}]$ $+ [Cr^{3+}] + [NO_3^-] = 0.2$ M). Then the mixed solution was titrated with 1.0 M NaOH up to pH 9.0 with vigorous stirring at room temperature. After 15 min, the resulting slurry was hydrothermally treated in a Teflon-lined stainless autoclave at 90°C for 13 h, followed by separated by centrifugation, washed and finally vacuum-dried at 60°C for 24 h. The exfoliation of ZnCr-LDH was achieved by vigorous shaking of LDHs sample (1 g L^{-1}) in the formamide under N_2 bubbling to avoid carbonate contamination, as reported previously.[2]

The anionic CdS nanosol was prepared as suggested by previous work with slight modifications.[36] Under the protection of N_2 atmosphere and constant stirring, a mixture of 2 mmol $Cd(NO_3)_2 \cdot 4H_2O$ and 2 mmol mercaptoacetic acid were

dissolved into 1000 mL deionized water, and the pH of the solution was then adjusted to 6.0 by the dropwise addition of 0.1 M NaOH. After 20 min, 80 mL of 0.025 M $Na_2S \cdot 9H_2O$ solution was slowly added. Finally, the resulting suspension was kept stirring overnight under N_2 environment before using. For comparison, the CdS precipitates were obtained by adding ethanol into the solution.

The self-assembled nanohybrid CdS/ZnCr-LDH was prepared by the dropwise addition of the mercaptoacetic acid-coated CdS nanosol (5.0×10^{-4} M) into the formamide suspension of ZnCr-LDH nanosheets (2.0×10^{-3} M) at room temperature. The molar ratio of CdS to ZnCr-LDH was 1:1. After stirring for 24 h, the mixed suspension was aged at 60°C for 24 h to ensure the completion of hybridization reaction. The resulting nanohybrid CdS/ZnCr-LDH was separated by centrifugation, washed with absolute ethanol and distilled water, and finally vacuum-dried at 60°C for 24 h. To prevent the contamination of the LDHs materials from carbonate ions, the preparation processes throughout were carried out with decarbonated water under CO_2-free N_2 atmosphere.

2.2 Characterization

Powder X-ray diffraction (XRD) patterns were collected at room temperature on a Rigaku SmartLab 3KW diffractometer using Cu Kα radiation (λ = 0.15418 nm). High-resolution transmission electron microscope (HRTEM) images using a JEOL JEM-2100 with an accelerating voltage of 300 kV. The samples were suspended in ethanol and sonicated over 10 min. Subsequently, a drop of the supernatant dispersion was placed onto a carbon film supported by a copper grid. UV-vis diffuse reflectance spectra (DRS) were recorded on a Shimadzu UV-2550 spectrophotometer equipped with a 60-mm integrating sphere using $BaSO_4$ as the reference. Specific surface area and porosity measurements were carried out on a Nova 1200e instrument at liquid-nitrogen temperature using ultrapure nitrogen gas as the adsorbate, in which all samples were degassed at 150°C for 4 h in flowing N_2 prior to the measurements. X-ray photoelectron spectroscopy (XPS) measurements were performed on a VG Escalab MK II spectrometer (Scientific Ltd.) with non-monochromatic Al K X-ray (1486.6 eV). The pressure in the chamber during the experiments was less than 10^{-6} Pa. The analyzer was operated at 20 eV pass energy with an energy step size of 0.1 eV. Electrochemical and photoelectrocatalytic measurements were carried out with a PAR 2273 potentiostat/ galvanostat using a conventional three-electrode cell. A Pt mesh and Ag/AgCl in saturated potassium chloride electrode (+0.198 V *vs* NHE) were used as the counter and reference electrodes, respectively. The working electrodes were prepared by pasting a uniform layer of material on indium-tin oxide (ITO) glass with an active area of ca. 0.75 cm[2], similar to the reported procedure.[3] The supporting electrolyte was 0.2 M Na_2SO_4 aqueous solution and a 300 W Xe lamp was used to excite the electrode surface.

2.3 Photocatalytic test

The photocatalytic activity of synthesized samples was evaluated by the hydrogen evolution from water at 22°C using a 300 W xenon lamp as the ultraviolet-visible light source. When the lamp was used as the visible-light source, a 420 nm cutoff filter was added. The photocatalytic reactions were carried out in a top-irradiation Pyrex vessel connected to a CEL-SPH2N gas-closed circulation system in vacuum (Aulight Tech Co. Ltd, Beijing). 0.1 g photocatalyst was dispersed with a constant stirring in a 100 mL aqueous solution containing 0.1 M Na_2S and 0.1 M Na_2SO_3 as sacrificial agents. Prior to irradiation, the reactor was sealed and then thoroughly degassed to completely remove air and to ensure the reaction system under anaerobic conditions. A continuous magnetic stirrer was applied at the bottom of the reactor in order to keep the photocatalyst particles in suspension status during the whole experiments. The evolved hydrogen amount was measured by an online gas chromatograph (Shimadzu GC7890II, thermal conductivity detector, 5Å molecular sieve columns and Ar carrier).

3. Results and discussion

3.1 Structural analyses

As shown in Fig. 1, the pristine ZnCr-LDH shows typical Bragg reflections of the hexagonal LDH phase with interlayer nitrate ions (JCPDS 38-0486). Its strong and sharp (00*l*) reflections suggest that the well-ordered layered structure was formed. After exfoliation in formamide, the resultant ZnCr-LDH nanosheets are positively charged. Derived from the electrostatic interactions, the negatively charged CdS nanosol particles were hybridized with the LDH nanosheets. The resultant CdS/ZnCr-LDH nanohybrid exhibits (00*l*) reflections at lower angles. The reflections at 3.54°, 8.25° and 16.82° can be indexed as (001), (002) and (003), and the interlayer spacing was determined to be 2.50 nm. Deducting from the thickness of the host sheet (0.48 nm),[25] the gallery height of CdS/ZnCr-LDH was determined to be 2.02 nm. The diffraction peaks at 26.5, 43.9 and 51.7°, attributed to the sphalerite CdS (JCPDS 10-0454), were distinctly observed. The in-sheet (110) peak of the hexagonal LDHs phase with a broad hump shape was also observed at ~60°, indicating the maintenance of the layer framework of ZnCr-LDH nanosheets. In the synthesis process, we employed different molar ratios of CdS to ZnCr-LDH (2:1, 1:1 and 1:2) under the same conditions to prepare CdS/ZnCr-LDH. It was found that their XRD patterns were very similar. Energy dispersive X-ray spectroscopy (Oxford 7021) gave a closely identical value of metal elements for each case. The CdS:ZnCr-LDH molar ratio of was (0.46±0.02):1. This observation implies that the loading of CdS for such a pillared structure is definite, which is dependant on the surface charge ratio of the guest CdS nanoparticle to the host LDHs nanosheet, similar to the previous report.[25]

The HRTEM images provided direct evidence for incorporating CdS into ZnCr-LDH interlayer. As illustrated in Fig. 2, the ZnCr-LDH nanosheets in a nanohybrid crystallite are parallel to each other. The vertical distance of the adjacent

sheets is about 2.5 nm, in agreement with the XRD results. The CdS pillars are observed to irregularly locate on the interlayer region of the host lattice. The ZnCr-LDH nanosheets and the CdS pillars have been integrated by the way of an intimated contact, which is expected to form a desirable heterostructure. The random aggregation of the intersected crystallites, forming the house-of-cards type stacking, leads to the formation of different voids.
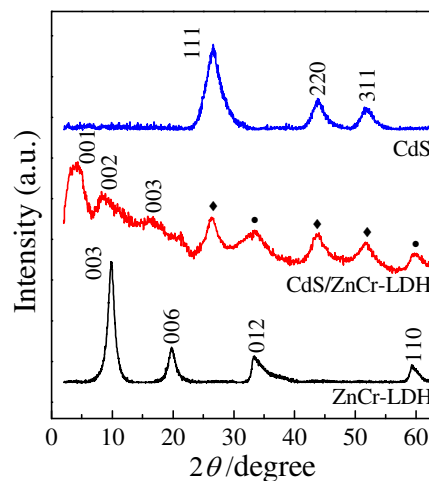

Fig. 1. Powder XRD patterns of ZnCr-LDH, CdS and CdS/ZnCr-LDH, where ♦ for CdS and ● for the in-sheet diffraction of ZnCr-LDH.
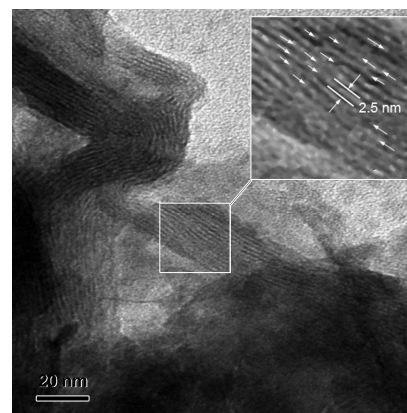

Fig. 2. Typical HRTEM image of CdS/ZnCr-LDH, where the white arrows indicate the CdS pillars between the host sheets.

The N_2 adsorption–desorption isotherms of CdS/ZnCr-LDH, ZnCr-LDH and CdS were investigated. As plotted in Fig. 3, the isotherm of CdS exhibits the characteristic of a typical microporous adsorbent with no distinct hysteresis. However, a distinct hysteresis is observable for CdS/ZnCr-LDH at $p/p_0 > 0.45$, indicating the presence of mesopores. The observed isotherm and hysteresis behaviors can be assigned as BDDT-type IV and IUPAC-H2 type hysteresis loop,[37,38] which is characteristic of mesoporous materials having a high energy of adsorption and the presence of well-ordered pores with narrow and wide sections and interconnecting channels. Such a type of isotherm and hysteresis reflects the presence of the open slit-shaped capillaries with very wide bodies and narrow short

necks.[25,38]

As plotted in the inset of Fig. 3, the pore-size distribution curve based on BJH method shows that the as-prepared nanohybrid is mesoporous with an average diameter of ~3.8 nm and a pore volume of 0.19 cm³g⁻¹ (Table S1 in Electronic Supplementary Information, ESI). The ~2.2 nm peak corresponds to the gallery height of 2.02 nm, determined from XRD. The ~3.8 nm peak with a wide pore distribution may be attributed to the formation of the house-of-cards stacking of layered crystallites, which has been encountered in the reported oxide-pillared titanates, niobates and tantalates.[29–31,39] The mesoporous texture results in that CdS/ZnCr-LDH possesses an expanded specific surface area of 86 m² g⁻¹, compared with that of the pristine ZnCr-LDH (33 m² g⁻¹).
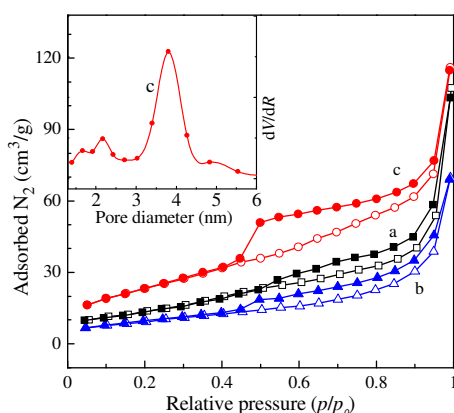

Fig. 3. Nitrogen adsorption–desorption isotherms of CdS (a), ZnCr-LDH (b) and CdS/ZnCr-LDH (c). The inset indicates the pore size distribution curve of CdS/ZnCr-LDH.
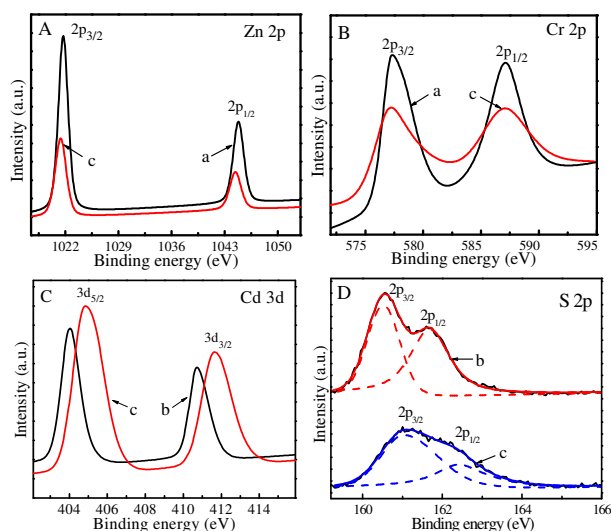

Fig. 4. XPS spectra of Zn 2p (A), Cr 2p (B), Cd 3d (C) and S 2p (D) in ZnCr-LDH (a), CdS (b) and CdS/ZnCr-LDH (c).

Fig. 4 shows the XPS spectra of Zn 2p, Cr 2p, Cd 3d and S 2p in materials and their corresponding binding energies are listed in Table S2. The data of pure CdS and the pristine ZnCr-LDH are in consistent with the previous reports.[3,27] Compared with the pristine ZnCr-LDH, the binding energies of Zn 2p and

Cr 2p in CdS/ZnCr-LDH show a slightly negative shift. On the contrary, the binding energies of Cd 3d, and S 2p in CdS/ZnCr-LDH display obvious shift to high energy, compared with CdS. These shifts should be attributed to the hybridization between the host and the guest, which contributes the electron transfer from CdS to ZnCr-LDH. The results suggest that there exists an electronic coupling between the ZnCr-LDH nanosheets and the CdS nanoparticles in such a host-guest heterostructure, which is beneficial to depress the photoinduced charge carries recombination during the photocatalytic reaction.

3.2 UV-Vis diffuse reflectance spectra and band structure determination

Fig. 5 shows the comparison of the UV-vis diffused reflectance spectra of the samples. the pristine ZnCr-LDH shows two strong absorption peaks at 2.2 and 3.0 eV corresponding to the d-d transitions of trivalent chromium ions.[2] The onset wavelength of CdS is 544 nm with the corresponding band gaps of 2.28 eV.[33] Upon the hybridization with the ZnCr-LDH, the resulting CdS/ZnCr-LDH nanohybrid also displays two strong absorption peaks at 2.10 and 2.32 eV, indicating an effective electronic coupling between CdS nanoparticles and the ZnCr-LDH nanosheets. The synergistic effect leads to a narrower band gap and then makes the electronic absorption onset red-shifted. The expanded absorption would harvest more photons than ZnCr-LDH and CdS to produce more photogenerated charge carriers, resulting in enhanced photocatalytic activity.
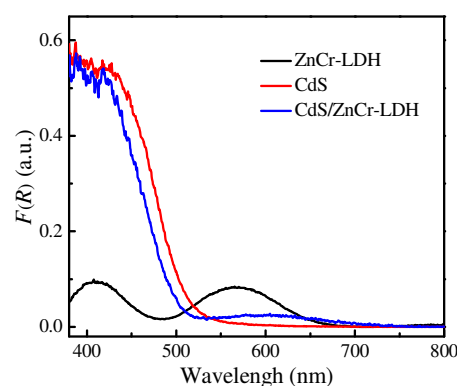

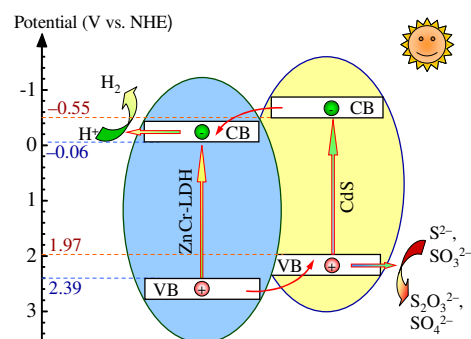**Fig. 5.** Diffuse UV-vis spectra of ZnCr-LDH, CdS, and CdS/ZnCr-LDH.

Fig. 6. Schematic model for the band structures of ZnCr-LDH and CdS.

To understand the electron transfer between ZnCr-LDH and

CdS, the band structures were estimated from the results of Mott-Schottky plots and DRS. The Mott-Schottky plots gave the corresponding low edge position of the conduction bands (CB) are −0.06 eV (Fig. S2). Therefore, the top edge of valence band (VB) for ZnCr-LDH can be determined 2.39 eV. Similarly, the low edge of CB for CdS was probed at the position of −0.55 eV, and its top edge of VB is positioned at 1.97 eV with a band gap of 2.52 eV. These measuring results are in good agreement with previous reports.[2,36] The band alignment of ZnCr-LDH and CdS in CdS/ZnCr-LDH is depicted in Fig. 6. The top edge of VB for CdS is higher than that of ZnCr-LDH, and its low edge of CB is higher than that of ZnCr-LDH. Upon light excitation, the photogenerated electrons in CdS can migrate into the CB of ZnCr-LDH, and the photogenerated holes transfer in the opposite direction and accumulate in the VB of CdS. Such spatial separation of electrons and holes can make contribution to the improvement of photocatalytic activity through depressing the electron-hole recombination.

3.3 Electrochemical and photoelectrochemical properties

The interface charge transfer process of photogenerated electrons and holes is a vital factor for photocatalytic activity, and it can be investigated by the typical electrochemical impedance spectra (EIS). Fig. 7 shows the Nyquist plots of the as-prepared samples. The semicircle of the curve on the EIS spectra reflects the interface layer resistance occurring at the surface of electrode, and the smaller curve semicircle reveals the lower impedance, which can help charge transfer easily. It is observed that the arc radius of CdS/ZnCr-LDH is much lower than those of ZnCr-LDH and CdS, indicating the efficient electron coupling of these two components in the heterostructured pillared system.
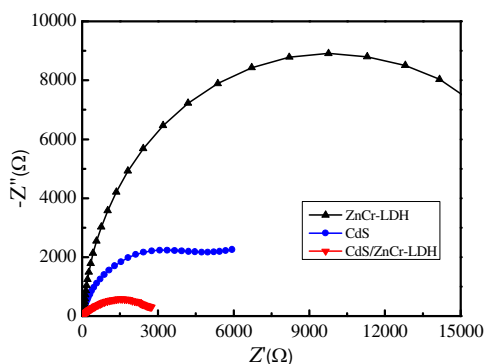

Fig. 7. Nynquist plots of ZnCr-LDH, CdS and CdS/ZnCr-LDH in 0.2 M Na$_2$SO$_4$ electrolyte.

In order to further investigate the electronic interaction between ZnCr-LDH and CdS, the photocurrent transient response measurements were performed under intermittent illumination. Fig. 8 shows the photocurrent responses for each switch-on/off operation for ZnCr-LDH, CdS and CdS/ZnCr-LDH photoanodes. It is clear that the photocurrent of the CdS/ZnCr-LDH electrode is much higher than that of the ZnCr-LDH and CdS electrodes, which is attributed to the efficient

electron coupling between ZnCr-LDH and CdS and consequently the significant enhancement of the separation and transfer efficiency of photogenerated electron-hole pairs.
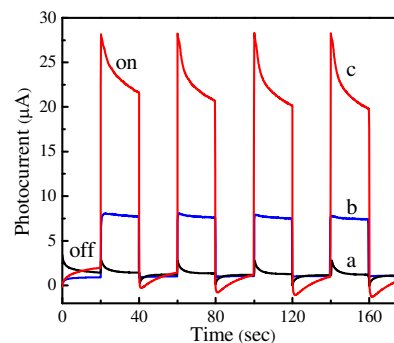

Fig. 8. The photocurrent-response of ZnCr-LDH (a), CdS (b) and CdS/ZnCr-LDH (c) in a 0.2 M Na$_2$SO$_4$ electrolyte under the irradiation of 300W Xe lamp.

3.4 Photocatalytic H$_2$ production

The photocatalytic activities of the investigated samples were evaluated by monitoring hydrogen evolution from water with 0.1 M Na$_2$S and 0.1 M Na$_2$SO$_3$ as the sacrificial agents under irradiation of visible and UV-visible light, respectively. Fig. 9 demonstrates the average results of 3 repeating experiments with an error bar for each case. CdS/ZnCr-LDH, prepared from the ratio of CdS to ZnCr-LDH being 1:1, shows remarkably improved photocatalytic hydrogen evolution, compared to ZnCr-LDH and CdS. The average H$_2$ evolution rate of CdS/ZnCr-LDH was 2164 μmol h^{-1} g^{-1} under UV-visible irradiation, which is about 16.9 times as high as ZnCr-LDH (128 μmol h^{-1} g^{-1}) and 2.2 times as high as CdS (966 μmol h^{-1} g^{-1}). Under the visible irradiation alone, the rate of H$_2$ production of CdS/ZnCr-LDH was 374 μmol h^{-1} g^{-1}, which is 1.7 times as high as CdS (216 μmol h^{-1} g^{-1}). As mentioned above, the intercalated loadings of CdS were closely identical with each other for the different nanohybrids prepared from different guest/host ratios. It was found that the different pillared nanohybrids have similar photocatalytic activity. As shown in Fig. S3, the evolution rates of the products prepared from CdS:ZnCr-LDH=1:2 and 2:1 were 1978 and 2067 μmol h^{-1} g^{-1} under UV-visible irradiation, and their photocatalytic activity under the visible irradiation were 345 and 362 μmol h^{-1} g^{-1}, respectively. The CdS:ZnCr-LDH ratio of 1:1 is optimal to prepare CdS/ZnCr-LDH nanohybrid with high photocatalytic activity. This condition may be propitious to form the close contact between the guest nanoparticles and the host nanosheets, which will improve their electronic coupling interactions.

The quantum efficiencies (QEs) for hydrogen generation was estimated using the reported procedure.[40] As summarized in Table S3, the QE for CdS/ZnCr-LDH is 48.2% under UV-visible light irradiation, which is higher than those of ZnCr-LDH (19.8%) and CdS (12.1%). Under the visible irradiation alone, the QEs for CdS/ZnCr-LDH, ZnCr-LDH and CdS are 42.6%, 2.4% and 9.1%, respectively. The enhancement of the photocatalytic activity of CdS/ZnCr-LDH, compared with its parents ZnCr-LDH and CdS, is attributed to the efficient

electronic coupling between its two components and also to the expanded surface area.
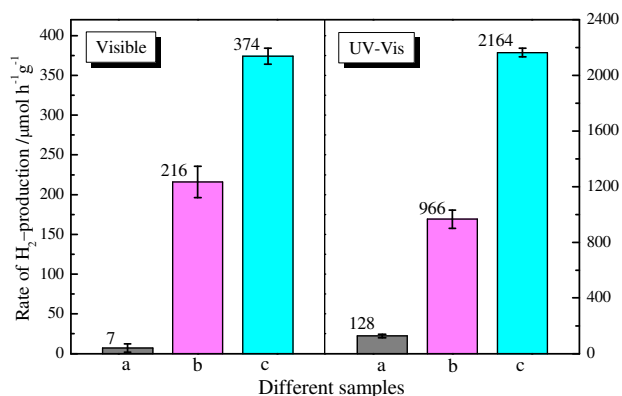

Fig. 9. Comparison of hydrogen evolution activity of ZnCr-LDH (a), CdS (b) and CdS/ZnCr-LDH (c) under irradiation of visible (left) and UV-visible light (right).

As shown in Fig. 6, upon the light irradiation, electrons in the VBs of ZnCr-LDH and CdS will be excited. The photogenerated CB electrons of the guest CdS nanoparticles can migrate through traversing the interface to the CB of the host ZnCr-LDH nanosheets. And the photogenerated VB holes of the host will shift to the VB of the guest. Subsequently, the photogenerated CB electrons of the host will transfer to the surface to reduce the absorbed H^+ to produce H_2; and the photogenerated holes of the guest will oxidize S^{2-}, SO_3^{2-} to $S_2O_3^{2-}$ and SO_4^{2-}.[41] Such spatial separation of photogenerated charges increases the lifetime of the photogenerated electron and hole at the cost of a small loss in potential energy as the electron moves out of the higher CB potential of CdS into the lower CB potential of ZnCr-LDH. Although this decreases the over potential for H^+ reduction, it can lead to an increase in efficiency as long as a sufficient over potential remains. With the increased lifetime of the photogenerated electron, there is an increased likelihood that the electron will reduce H^+ before its back-recombination with the hole in CdS can occur, which leads to the improvement in photocatalytic activity. Comparing the activities, one can find that the H_2 evolution rate under UV-visible irradiation is higher than that under visible irradiation for each photocatalyst. This is attributed to that fact that the UV-visible irradiation can provide more photons to excite the VB electrons in the materials to induce the formation of the photogenerated electrons and holes. Additionally, it is well-known that heterogeneous photocatalysis is a surface-controllable process.[1] The expanded specific surface area of CdS/ZnCr-LDH, compared with ZnCr-LDH and CdS, contributes to its enhanced photocatalytic activity. However, it should be pointed out that the electronic coupling between the host ZnCr-LDH nanosheets and the guest CdS nanoparticles plays a crucial role in the hydrogen evolution from water splitting. The activities per area of CdS/ZnCr-LDH under UV-visible irradiation and under visible irradiation are 25.16 and 4.35 µmol h^{-1} cm^{-2} respectively, whereas the activities are 3.88

and 0.21 µmol h^{-1} cm^{-2} for ZnCr-LDH, and 10.05 and 2.92 µmol h^{-1} cm^{-2} for CdS.

Cadmium sulfide always shows declination in their photocatalytic activities due to photocorrosion.[4,8] The photocatalytic performance of CdS/ZnCr-LDH was examined with repeated photoreactions for three cycles under visible and UV-visible irradiation, respectively. No obvious activity drop was observed in our experiments (Fig. S4), clearly demonstrating that the as-prepared nanohybrid has good stability and recycling performance.

4. Conclusions

In this work, electrostatically derived incorporation of CdS into ZnCr-layered double hydroxide interlayer yielded mesoporous CdS/ZnCr-LDH nanohybrid, which exhibits an excellent photocatalytic activity for H_2 generation under irradiation of visible and UV-visible light. The remarkably improved photocatalytic activity of the as-present nanohybrid is attributed not only to the formation of highly porous texture with an expanded surface area but also to the strong electronic coupling between the two components, resulting in the depression of photogenerated charge carriers. The photocatalytic activity of the present nanohybrid were 374 µmol·h^{-1}·g^{-1} with a QE of 42.6% and 2164 µmol·h^{-1}·g^{-1} with a QE of 48.2% under visible and UV-visible irradiation, respectively, which is much higher than those of the parents ZnCr-LDH and CdS. The present findings clearly highlight that the self-assembly of LDH-CdS nanohybrid is quite effective in synthesizing novel porous photocatalyst with high photocatalytic efficiency and improved chemical stability in the hydrogen generation from water splitting.

Acknowledgments

References

1   X. B. Chen, S. H. Shen, L. J. Guo and S. S. Mao, *Chem. Rev.*, 2010, **110**, 6503-6570.

2   J. L. Gunjakar, T. W. Kim, H. N. Kim, I. Y. Kim and S.-J. Hwang, *J. Am. Chem. Soc.*, 2011, **133**, 14998–15007.

3   B. Zhu, B. Lin, Y. Zhou, P. Sun, Q. Yao, Y. Chen and B. Gao, *J. Mater. Chem. A*, 2014, **2**, 3819–3827.

4   Q. Li, B. Guo, J. Yu, J. Ran, B. Zhang, H. Yan and J. R. Gong, *J. Am. Chem. Soc.*, 2011, **133**, 10878–10884.

5   N. Z. Bao, L. M. Shen, T. Takata, and K. Domen, *Chem. Mater.*, 2008, **20**, 110–117.

6   L. N. Silva, S. Y. Ryu, J. Choi, W. Choi and M. R. Hoffmann, *J. Phys. Chem. C*, 2008, **112**, 12069–12073.

7   J. F. Reber and M. Rusek, *J. Phys. Chem.*, 1986, **90**, 824–834.

8   A. Vaneski, J. Schneider, A. S. Susha and A. L. Rogach, *J. Photochem. Photobiol. C*, 2014, **19**, 52–61.

9   W.-T. Chen, T.-T. Yang and Y.-J. Hsu, *Chem. Mater.*, 2008, **20**, 7204–7206.

10 Y. Li, Y. Xie, S. Peng, G. Lu and S. Li, *Chemosphere*, 2006, **63**, 1312–1318.

11 X. Li, Y. Jia and A. Cao, *ACS Nano*, 2009, **4**, 506–512.

12 Z.Y. Ren, J. Y. Zhang, F. X. Xiao and G. C. Xiao, *J. Mater. Chem. A*, 2014, **2**, 5330–5339

13 L. Sheeney-Haj-Ichia, B. Basnar and I. Willner, *Angew. Chem., Int. Ed.*, 2005, **44**, 78–83.

14 D. R. Baker and P. V. Kamat, *Adv. Funct. Mater.*, 2009, **19**, 805–811.

15 L. Jia, D. H. Wang, Y. X. Huang, A. W. Xu and H. Q. Yu, *J. Phys. Chem. C*, 2011, **115**, 11466–11473.

16 H. N. Kim, T. W. Kim, I. Y. Kim and S. J. Hwang, *Adv. Funct. Mater.*, 2011, **21**, 3111–3118.

17 Q. Wang and D. O'Hare, *Chem. Rev.*, 2012, **112**, 4124-4155.

18 K. J. Martin and T. J. Pinnavaia, *J. Am. Chem. Soc.*, 1986, **108**, 541–542.

19 T. J. Pinnavaia, *Science*, 1983, **220**, 365–371.

20 G. Centi and S. Perathoner, *Microporous Mesoporous Mater.*, 2008, **107**, 3–15.

21 N. Baliarsingh, L. Mohapatra and K. Parida, *J. Mater. Chem. A*, 2013, **1**, 4236–4243.

22 C. G. Silva, Y. Bouizi, V. Fornés and H. García, *J. Am. Chem. Soc.*, 2009, **131**, 13833–13839.

23 Y. Zhao, B. Li, Q. Wang, W. Gao, C. J. Wang, M. Wei, D. G. Evans, X. Duan and D. O'Hare, *Chem. Sci.*, 2014, **5**, 951.

24 J. L. Gunjakar, I. Y. Kim, J. M. Lee, N.-S. Lee and S.-J. Hwang, *Energy Environ. Sci.,* 2013, **6**, 1008–1017.

25 J. L. Gunjakar, T. W. Kim, I. Y. Kim, J. M. Lee and S.-J. Hwang, *Sci. Rep.*, 2013, **3**. 2080.

26 B. Li, Y. Zhao, S. Zhang, W. Gao and M. Wei, *ACS Appl. Mater. Interf.*, 2013, **5**, 10233–10239.

27 K. Parida and L. Mohapatra, *Dalton Trans.*, 2012, **41**, 1173–1178.

28 K. M. Parida, M. Satapathy and L. Mohapatra, *J. Mater. Chem.*, 2012, **22**, 7350–7357.

29 X. Fan, B. Lin, H. Liu, L. He, Y. Chen and B. Gao, *Int. J. Hydrogen Energy*, 2013, **38**, 832–839.

30 T. W. Kim, S. G. Hur, S. J. Hwang, H. Park, W. Choi and J. H. Choy, *Adv. Funct. Mater.*, 2007, **17**, 307–314.

31 X. T. Pian, B. Z. Lin, Y. L. Chen, J. D. Kuang, K. Z. Zhang and L. M. Fu, *J. Phys. Chem. C,* 2011, **115**, 6531–6539.

32 Q. L. Wu, A. Olafsen, Ø. B. Vistad, J. Roots and P. Norby, *J. Mater. Chem.*, 2005, **15**, 4695–4700.

33 W. Shangguan and A. Yoshida, *J. Phys. Chem. B*, 2002, **106**, 12227-12230

34 X. Xu, F. Zhang, S. Xu, J. He, L. Wang, D. G. Evans and X. Duan, *Chem. Commun.*, 2009, 7533-7535.

35 Z. An, S. Lu, L. Zhao and J. He, *Langmuir*, 2011, **27**, 12745–12750.

36 J. Zheng, F. Huang, S. Yin, Y. Wang, Z. Lin, X. Wu and Y. Zhao, *J. Am. Chem. Soc.*, 2010, **132**, 9528–9530.

37 J. B. Condon, *Surface Area and Porosity Determinations by Physisorption: Measurements and Theory*, Elsevier: Amsterdam; Boston, 2006.

38 S. J. Gregg and K. S. Sing, *Adsorption, Surface Area and Porosity*, Academic Press, London, 2nd edn, 1983.

39 X. L. Li, B.Z. Lin, B. H. Xu, Z. J. Chen, Q. Q. Wang, J. D. Kuang and H. Zhu, *J. Mater. Chem.*, 2010, **20**, 3924–3931.

40 R. Asahi, T. Morikawa, T. Ohwaki, K. Aoki and Y. Taga, *Science*, 2001, **293**, 269–271

41 Z. B. Yu, Y. P. Xie, G. Liu, G. Q. M. Lu, X. L. Ma and H. M. Cheng, *J. Mater. Chem. A,* 2013, **1**, 2773–2776.

Highly efficient photocatalytic hydrogen generation by incorporating CdS into ZnCr-layered double hydroxide interlayer

Guohua Zhang, Bizhou Lin,* Weiwei Yang, Shaofeng Jiang, Qianru Yao, Yilin Chen and Bifen Gao

Contents Entry
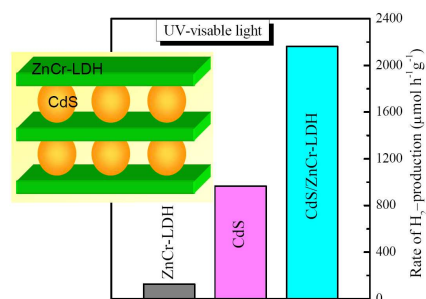
Incorporating CdS nanoparticles into the interlayer of ZnCr-LDH nanosheets led to the formation of CdS-pillared ZnCr-LDH nanohybrid, which exhibited superior photocatalytic hydrogen-generation performance from water splitting due to the strong electronic coupling between its two components.